Yersinia actively downregulates type III secretion and adhesion at higher cell densities

Francesca Ermoli[1], Christoph Spahn[2], Timo Glatter[3] & Andreas Diepold[1]

1: Max Planck Institute for Terrestrial Microbiology, Department of Ecophysiology, Marburg, Germany

2: Max Planck Institute for Terrestrial Microbiology, Department of Natural Products in Organismic Interactions, Marburg, Germany

3: Max Planck Institute for Terrestrial Microbiology, Core Facility for Mass Spectrometry and Proteomics, Marburg, Germany

Corresponding author:

Andreas Diepold, andreas.diepold@mpi-marburg.mpg.de, +49-6421-178302

Short title: *Yersinia* downregulates type III secretion and adhesion at higher densities

Abstract

The T3SS injectisome is used by Gram-negative bacteria, including important pathogens, to manipulate eukaryotic target cells by injecting effector proteins. Some bacterial species display bimodal expression of the T3SS, allowing the T3SS-negative population to benefit from the activity of their T3SS-positive siblings without investing in the assembly and production of injectisomes. In contrast, *Yersinia enterocolitica*, a main T3SS model organism that uses the system to evade the host immune response, was thought to uniformly express and assemble injectisomes, which are then activated by target cell contact. In this study, we found that at higher local bacterial concentrations, *Yersinia* actively downregulates T3SS expression, assembly and activity. This effect is reversible, highly specific, and distinct from stationary phase adaptation. A key player is the main T3SS transcription factor VirF, which is downregulated at the higher cell densities suppressing T3SS activity and whose *in trans* expression restores T3SS expression and assembly. Transcript analysis showed that this effect is mediated by increased levels of the regulatory RNAs *csrBC*, which sequester the regulatory protein CsrA and destabilize the *virF* transcript. Downregulation of the VirF-dependent adhesin YadA led to a drastic reduction in bacterial cell adhesion. We propose that the phenotype described in this study, active downregulation of cell attachment and T3SS secretion at higher local bacterial densities, is a strategy implemented to promote bacterial replication and dissemination at later stages of infection.

Introduction

To manipulate eukaryotic cells, many Gram-negative bacteria, including important human pathogens, use a type III secretion system, which allows to inject effector proteins into target cells in a one-step mechanism [1–4]. These effector proteins can exert a wide variety of functions that facilitate survival and proliferation of the respective bacteria according to their infection route and lifestyle [5–7]. In contrast, the T3SS machinery, also known as injectisome, is highly conserved. It consists of a set of ring structures that anchor the injectisome in the bacterial membranes and surround an export apparatus in the inner membrane (IM), thought to act as a gating structure [8,9]. A hollow needle structure forms a conduit for the effectors, which is connected to a translocon pore in the target cell membrane (Fig. 1a). At the cytosolic interface of the injectisome, a set of conserved cytosolic components form six pod structures [10–14] that shuttle effectors between the injectisome and the cytosol in *Yersinia enterocolitica* [15–17].

Expression, assembly and activity of the T3SS are tightly regulated. Often, expression and assembly only occur within the host organism. In *Yersinia*, this is based on an RNA thermometer structure in the transcript of the main transcriptional activator of the T3SS, called VirF in *Y. enterocolitica* and LcrF in *Y. pseudotuberculosis* and *Y. pestis* [18,19]. While expression of VirF is sufficient for the formation of injectisomes, a second signal, host cell contact, is required to activate secretion. This activation, which can be mimicked by Ca^{2+} depletion in *Yersinia*, also removes the secreted posttranscriptional repressors YscM1/2 (LcrQ in *Y. pseudotuberculosis*) [20,21], leading to an upregulated production of the structural components and especially effectors of the system [21–23]. Recent studies in *Y. pseudotuberculosis* revealed additional layers of regulation (reviewed in [24]), such as the CsrABC system, where CsrA, which positively regulates T3SS expression by stabilizing the *virF* transcript, is sequestered by the two regulatory RNAs *csrB* and *csrC* [25].

This tight regulation of T3SS expression and activity may be required because of a phenomenon called secretion-associated growth inhibition (SAGI), in which secreting bacteria greatly reduce their growth and division. It was this striking phenotype that initially led to the discovery of the T3SS, when researchers noted a specific growth inhibition of virulent *Yersinia* (now known to be equivalent to the presence of the T3SS) at 37°C (T3SS expression) in the absence of Ca^{2+} (T3SS activation) [26–31]. Besides *Yersinia*, SAGI has been shown to occur in two other main T3SS model organisms, *Salmonella enterica* and *Shigella flexneri* [32–34]. However, it is still unclear if SAGI is a mere consequence of the energy expenditure for synthesis and export of the T3SS machinery and effectors, or whether it is an actively regulated phenotype, as suggested by the fact that growth and division are reinitiated very quickly, once secretion is stopped [35].

Given that the propagation of actively secreting bacteria is impeded, a bimodal distribution of T3SS expression is conceivably beneficial in some situations. Indeed, it was shown that the SPI-1 T3SS, used by *Salmonella enterica* to induce a strong inflammation in the host gut that clears competing bacteria, is only active in a subset of bacteria, allowing the T3SS-inactive subpopulation to rapidly populate the infection

niche [32,36]. Similarly, *Pseudomonas aeruginosa* expresses its T3SS in a bistable way [37–40]. In contrast, *Shigella flexneri* and *Yersinia enterocolitica*, where presence of the T3SS mainly gives a benefit to individual cells (invasion of the cytosol of epithelial cells and evasion of the immune response, respectively) [35,41], were so far found to be completely T3SS-positive, both in terms of expression and assembly of injectisomes [40,42–44] and their activation [45].

However, these results were gained under standard laboratory conditions typically focusing on the establishment of an infection at low bacterial densities. It is conceivable that this picture changes under conditions mimicking later stages of infection, where bacteria may benefit from suppressing T3SS assembly and activity, allowing them to replicate in their established niches or disseminate. Increased local bacterial density, a common aspect of later-stage infection environments, might therefore influence the activity of the T3SS.

In this study, we tested this hypothesis and found that at densities higher than under standard laboratory conditions, *Yersinia* actively downregulate the expression, assembly and activity of their T3SS and the coregulated adhesion factor YadA. This effect is reversible, highly specific, and distinct from stationary phase adaptation. Under these conditions, a >10 times increased concentration of the regulatory RNA *csrC* leads to sequestration of the RNA-binding protein CsrA and downregulation of expression of the main T3SS transcription factor VirF. Accordingly, expression of VirF *in trans* overrides the effect. We propose that the highly specific T3SS regulatory phenotype discovered in this study increases the chances of bacterial dissemination during and after infection by creating a T3SS-negative, non-adhesive subpopulation that can replicate and disseminate.

Results

Type III assembly and activity are affected by bacterial cell density

To investigate the interplay between type III secretion and local bacterial densities, we tested the effector secretion of *Y. enterocolitica* incubated under secreting conditions (37°C, low [Ca^{2+}]) at increasing cell densities. As *Y. enterocolitica* can reach optical densities at 600 nm (OD_{600}) of 15-20, the ODs at the inoculum (OD_{in}) used in this experiment correspond to the exponential phase growth in non-secreting bacteria (Suppl. Fig. 1). Cultures inoculated to an initial OD_{600} of 0.1 (OD_{in}=0.1), a condition regularly used for secretion experiments [40,45–47], which we refer to as reference hereafter, secreted large amounts of effector proteins. Increasing densities gradually reduced secretion levels, up to a complete inhibition of T3SS function at higher bacterial densities (OD_{in}=1.5) (Fig. 1B). This establishes an inverse correlation between T3SS secretion and cell density. To describe this unexpected phenotype in more detail, we next tested T3SS activation over time by quantifying the translation of the effector YopE, which is strongly upregulated upon T3SS activation [45,46,48]. To ensure a high sensitivity and temporal resolution, we used the fast-folding fluorescent protein sfGFP with a SsrA degradation tag [49] as a reporter. The resulting P_{yopE}-*sfGFP-ssrA* reporter system allowed for accurate temporal mapping of T3SS activation (Suppl. Fig. 2). In line with the previous results, the reporter showed a weaker and shorter T3SS activation with increasing bacterial densities, again up to a complete loss of activation at higher densities (Fig. 1C, Suppl. Fig. 3). To determine whether already the assembly of the T3SS machinery was impacted by cell density, the number of injectisomes was quantified by fluorescence microscopy at a single-cell level in a strain expressing a functional EGFP-SctQ fusion [42] (Fig. 1D). The analysis showed a significant reduction in the number of fluorescent foci corresponding to assembled injectisomes at all conditions tested when compared to the reference. Like protein secretion itself (Fig. 1B), T3SS assembly was almost fully repressed at higher cell densities. As expected, a certain degree of heterogeneity was observed under all conditions tested, but neither a bimodal distribution, nor distinct subpopulations were observed for T3SS activation or assembly (Fig. 1D, Suppl. Fig. 4), indicating a general downregulation of the T3SS. The results highlight a clear inverse correlation between cell density and T3SS assembly and activation, which we refer to as density-dependent downregulation of the T3SS (d^3T3).

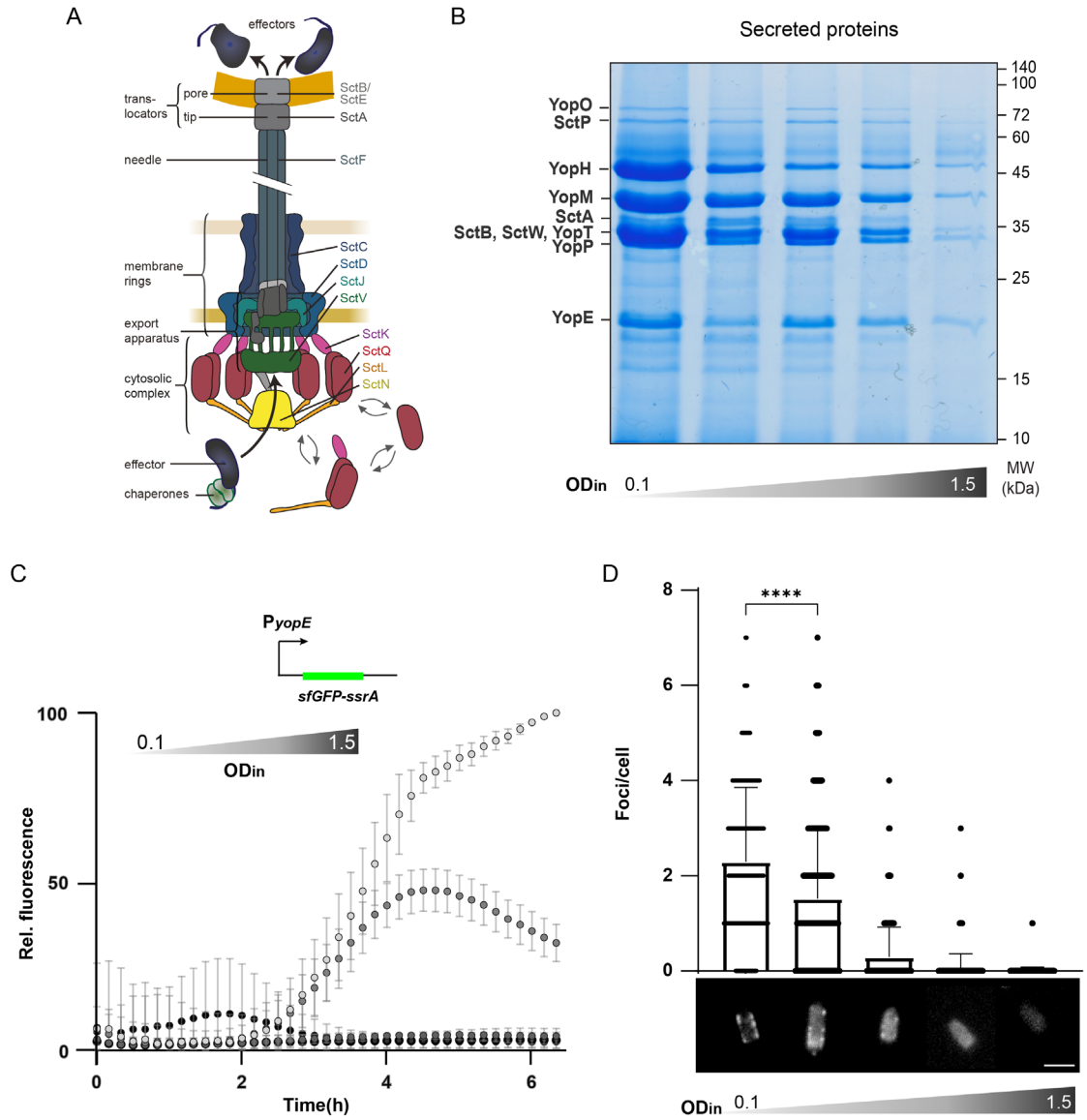

Fig. 1 – Assembly and activity of the T3SS are significantly reduced at higher bacterial densities.

A) Schematic depiction of the T3SS injectisome (adapted from [50]); right, common nomenclature names of main T3SS components [51,52]. B) Secretion assay displaying the effectors secreted by the T3SS (left) at increasing OD_{in} (left to right: 0.1, 0.3, 0.7, 1.0, 1.5). C) T3SS reporter assay using a strain expressing sfGFP-SsrA under the control of the *yopE* promoter, which is strongly upregulated upon T3SS activation [45,53], at increasing OD_{in} values as in B). *n=3*, whiskers denote standard deviation. Growth curves of cultures used in these experiments are displayed in Suppl. Fig. 5. D) Quantification of EGFP-SctQ foci per bacterium, corresponding to assembled injectisomes, visualized by fluorescence microscopy at increasing OD_{in} as in B). Sample micrographs depicted at bottom, scale bar, 2 µm. *n*=3 for all panels, gel image in B shows representative result. ***, $p < 0.0001$, whiskers denote standard deviation.

The density-dependent T3SS inhibition is specific and reversible

To probe if the observed correlation between bacterial density and the T3SS is specific or part of a more global regulatory effect, we compared the total proteome of bacteria with OD_{in}=1.5 to the reference (OD_{in}=0.1) (Fig. 2A). Remarkably, 32 of the 50 most strongly downregulated proteins were directly T3SS-related (machinery components, effectors, chaperones, see Suppl. Fig. 6), showing that the effect is highly specific for the T3SS. All T3SS proteins (marked by red dots in Fig. 2A) were highly downregulated (3-256-fold, p<0.001 for all detected components), except for the negative regulators YscM1 and YscM2, which were upregulated, and their chaperone SycH, whose expression remained stable (Fig. 2A, Table 1). The T3SS-associated trimeric adhesin YadA was similarly downregulated, whereas other proteins encoded on the pYV virulence plasmid were largely unaffected (Suppl. Table 1). This indicates that the downregulation is not caused by a change in plasmid copy number or overall protein expression from the plasmid. Instead, it suggests a direct effect of bacterial densities on T3SS expression that is distinct from stationary phase responses occurring at higher densities. In line with this interpretation, proteins involved in stationary phase response, which are highly expressed at stationary phase, were not significantly upregulated at OD_{in}=1.5 (Suppl. Table 2). In contrast, all T3SS gene classes – structural components, regulators, effectors and chaperones – were similarly affected (Suppl. Fig. 6, Table 1). Taken together, our data unanimously point towards a specific T3SS repression mechanism driven by cell density rather than a broader cellular reorganization.

We next tested if the d^3T3 effect is reversible. Bacterial cultures were inoculated at reference or higher OD (OD_{in}=0.1 or 1.5) and then concentrated or diluted to the OD of the respective other culture prior to induction of T3SS expression by a temperature shift to 37°C. Activation of the T3SS was quantified using the P_{yopE}-*sfGFP-ssrA* reporter described earlier. Increasing the density of initially dilute cultures strongly suppressed T3SS activation. Likewise, diluting the initially more concentrated cultures almost completely restored T3SS activation (Fig. 2B). We also tested a possible role of the medium composition (e.g. by limitation of nutrients or presence of extracellular negative regulators at higher densities) and found that secretion was neither suppressed at low density by spent medium from high-density cultures, nor activated at high densities by fresh medium (Fig. 2C). Together, these results highlight a direct and reversible influence of bacterial density on T3SS secretion.

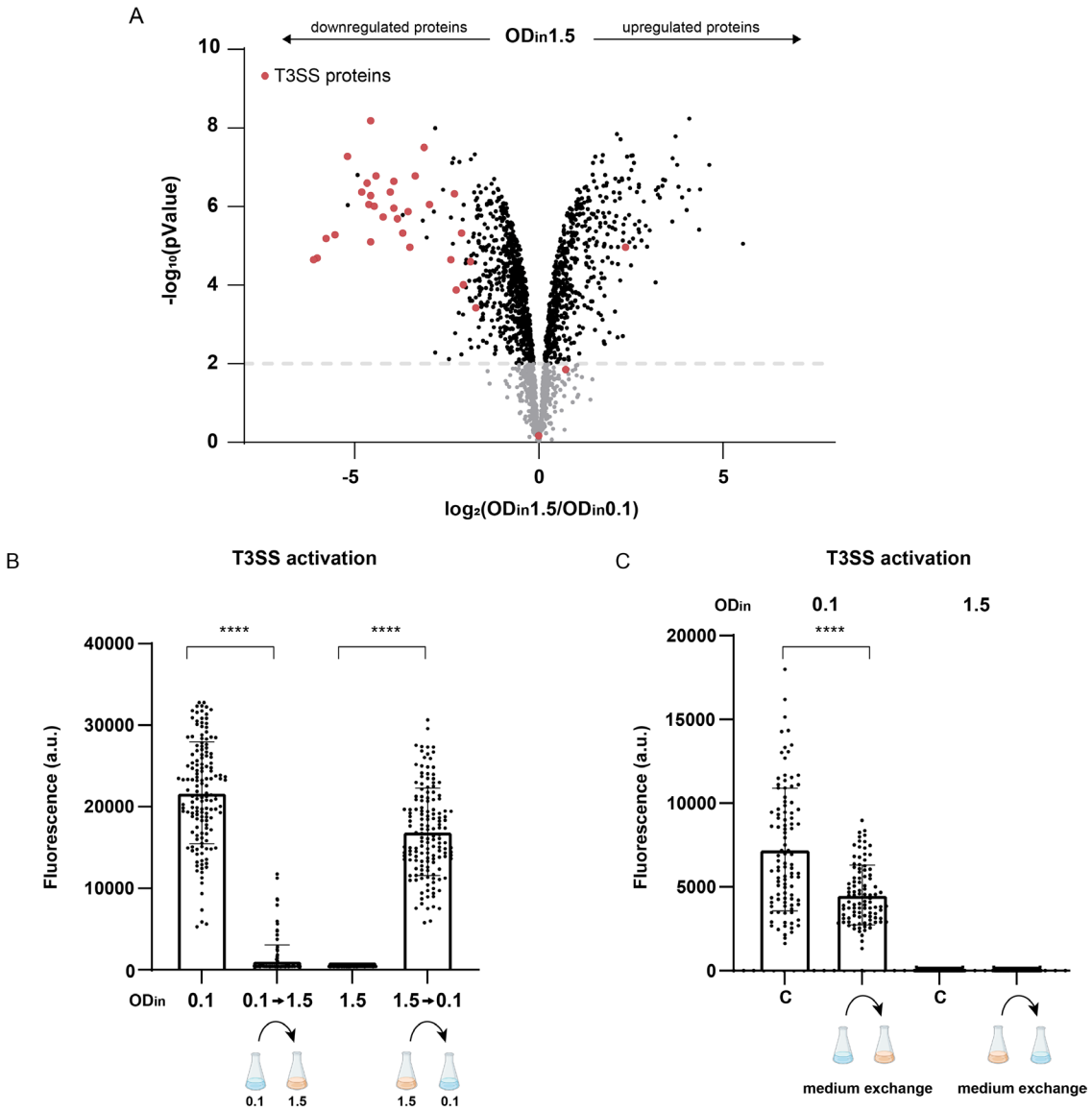

Fig. 2 – The density-dependent downregulation of the T3SS is specific and reversible.

A) Volcano plot showing differences in the expression of *Y. enterocolitica* proteins between cultures grown under secreting conditions at OD_{in} 1.5 and 0.1. All proteins with at least three detected peptides are displayed; T3SS-related proteins are marked by larger red dots. B) T3SS reporter assay (P_{yopE}-*sfGFP-ssrA*, see Fig. 1B for details) in strains with OD_{in} values and concentration or dilution at the time of the temperature shift to 37°C, as indicated. Measurements were performed 150 min after dilution/concentration. ****, $p<0.0001$, whiskers denote standard deviation. C) T3SS reporter assay (P_{yopE}-*sfGFP-ssrA*) in strains with OD_{in} values as indicated. Medium exchange at the time of the temperature shift to 37°C, as depicted; C stands for constant incubation without medium change. Measurements were performed 150 min after medium exchange. ****, $p<0.0001$, whiskers denote standard deviation. $n=3$ biological replicates for all panels.

Global stationary phase regulators have a minor effect on T3SS assembly and function

We next aimed to determine the cause for this previously unknown regulatory phenotype. To investigate a possible role of density-dependent global regulators of bacterial physiology and behavior in the density-dependent downregulation of the T3SS, we studied the influence of quorum sensing (QS) and the stationary phase/stress response alternative sigma factor RpoS [54,55]. In *Yersinia*, both a LuxI/R (*yenI/R*) and a LuxS homolog have been characterized, although no clear evidence of functional LuxS-dependent AHL-2 signaling has been provided so far. While QS in *Yersinia* influences, among others, motility and biofilm formation [56–58], its role in bacterial virulence is less clear. We performed a secretion assay in a *Y. enterocolitica* QS double mutant (Δ*yenI*,*lsrK*). The secretion pattern of the mutant showed no significant impact of QS on secretion at the conditions tested (Fig. 3A, Suppl. Fig. 7). Next, we tested the influence of the stationary phase/stress response sigma factor RpoS on d^3T3. RpoS is known to positively regulate motility and biofilm formation in many Gram-negative bacteria [54,55], but its impact on *Yersinia* virulence is unclear. The activity of the T3SS at OD_{in} 0.1 and 1.5 was not influenced by the deletion or overexpression of the RNA polymerase sigma factor RpoS (Fig. 3B).

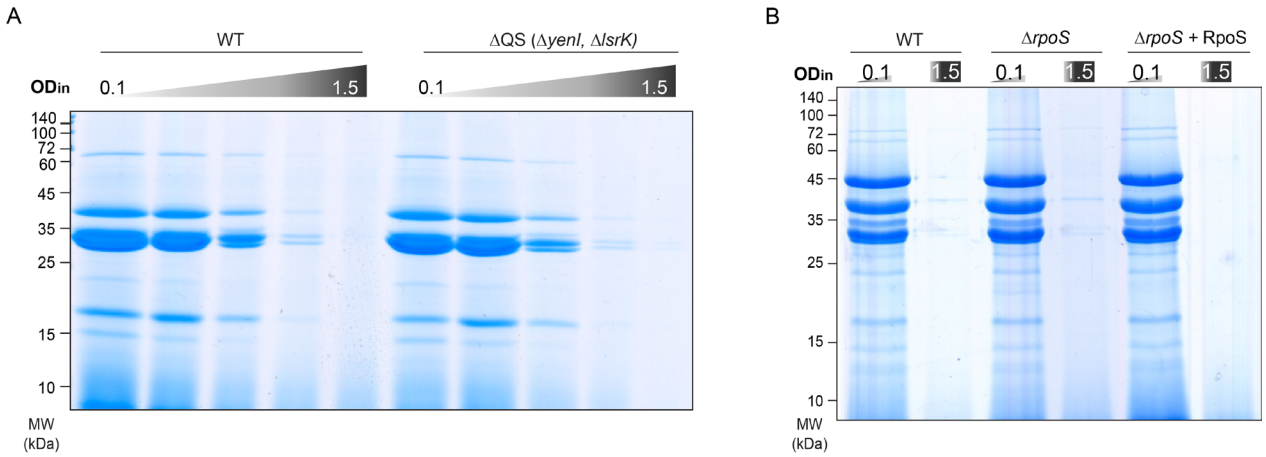

Fig. 3 – Quorum sensing and the alternative sigma factor RpoS do not significantly contribute to the density-dependent downregulation of the T3SS.

A) Secretion assay of wild-type (WT) and quorum sensing mutant strains at different OD_{in} as used in Fig. 1 (left to right, OD_{in} = 0.1, 0.3, 0.7, 1.0, 1.5). B) Secretion assay of the indicated strains at OD_{in} 0.1 and 1.5, as displayed. For *in trans* complementation of the *rpoS* mutant from pBAD::RpoS, RpoS expression was induced by the addition of 0.2% arabinose at the time of the shift to 37°C. *n*=3, gel images show representative results.

The transcriptional regulator VirF is the main target of the density-dependent T3SS regulation

Based on the specificity of the d^3T3 (Fig. 2A), the uniform influence on all T3SS components (Table 1, Suppl. Fig. 6), and the limited role of the tested global regulators (Fig. 3), we hypothesized the target of the repression to be a general regulator of the system. T3SS assembly and activation are controlled mainly by the AraC-like transcriptional activator VirF (Fig. 4A). In the absence of VirF, the *Yersinia* T3SS is inactive and its components are strongly repressed [19,59,60] (Suppl. Fig. 8). VirF was among the genes that were significantly downregulated at high cell densities (-12.64-fold, $p<10^{-5}$, Table 1). To test if this downregulation is a central factor for the d^3T3, we expressed VirF from a plasmid at OD_{in}=1.5. Additional expression of VirF was indeed sufficient to restore the T3SS activity (Fig. 4B), indicating that T3SS repression at higher cell densities largely is a consequence of reduced VirF levels.

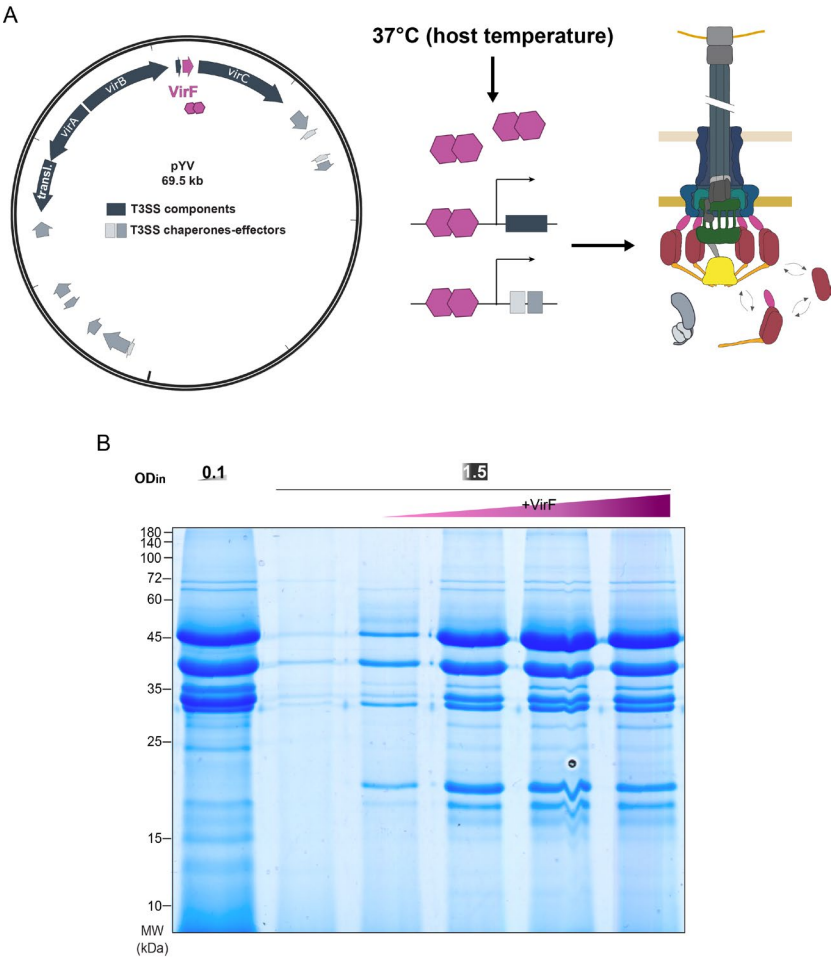

Fig. 4 – Additional expression of the transcriptional regulator VirF at higher densities restores T3SS secretion.

A) Schematic display of the genes encoding for T3SS structural components (operons *virA*, *virB*, *virC*, and translocator operon (transl.), dark grey), T3SS effectors and chaperones (lighter shades of grey), and VirF (purple) on the pYV virulence plasmid (left), and the principle working mechanism of VirF (right). B) Secretion assay showing effector secretion at OD_{in} = 0.1 (left) and 1.5 (right). Lanes 3-6, increasing expression of VirF *in trans* (arabinose concentrations of 0.001, 0.003, 0.008, 0.03%, respectively). *n*=3, gel image displays representative result.

Bacterial density influences VirF levels at a post-transcriptional level via the CsrABC pathway

We next investigated how cell density influences VirF levels. VirF is encoded in the *sctG-virF* operon (Fig. 5A). *sctG* encodes the pilotin protein, which assists the assembly of the T3SS secretin ring in the OM [61,62], but also has additional post-assembly functions [63]. Interestingly, it is the only T3SS component whose expression is largely VirF-independent [18,19,64]. Total proteome analysis and immunoblots showed SctG to be significantly less affected by higher cell densities than VirF or other T3SS components (Fig. 5B, Suppl. Fig. 9, Table 1). Fluorescence microscopy confirmed this on a single-cell basis (Fig. 5C). These results indicate that the regulatory region directly upstream of *virF*, rather than the promoter of the *sctG-virF* operon, is the target of d^3T3. To discriminate between transcriptional and post-transcriptional regulation, we measured the transcript abundance of *sctG* and *virF* by q-PCR. Mirroring the expression data, *virF* transcript levels were more strongly reduced by higher densities than *sctG*, pointing towards a cell density-driven post-transcriptional targeting of the *virF* mRNA (Fig. 5D). A known regulator of *virF* transcript abundance is the CsrABC pathway. In *Yersinia*, CsrA modulates T3SS activation via *virF* transcript regulation. CsrA binds to the *sctG-virF* mRNA intergenic region as a dimer, stabilizing the *virF* transcript by reducing its turnover rate [47,65] (Fig. 5E). The two regulatory non-coding RNAs *csrB* and *csrC* (Suppl. Fig. 10) sequester CsrA, preventing it from binding and stabilizing the *virF* transcript. To investigate a possible involvement of the CsrABC system in the d^3T3, we measured *csrB* and *csrC* levels at different densities and observed a significant upregulation of *csrB* and especially *csrC* at higher bacterial densities (Fig. 5F), suggesting that the subsequent increased sequestration of CsrA by *csrC* underlies the *virF* downregulation that causes d^3T3 at higher bacterial densities.

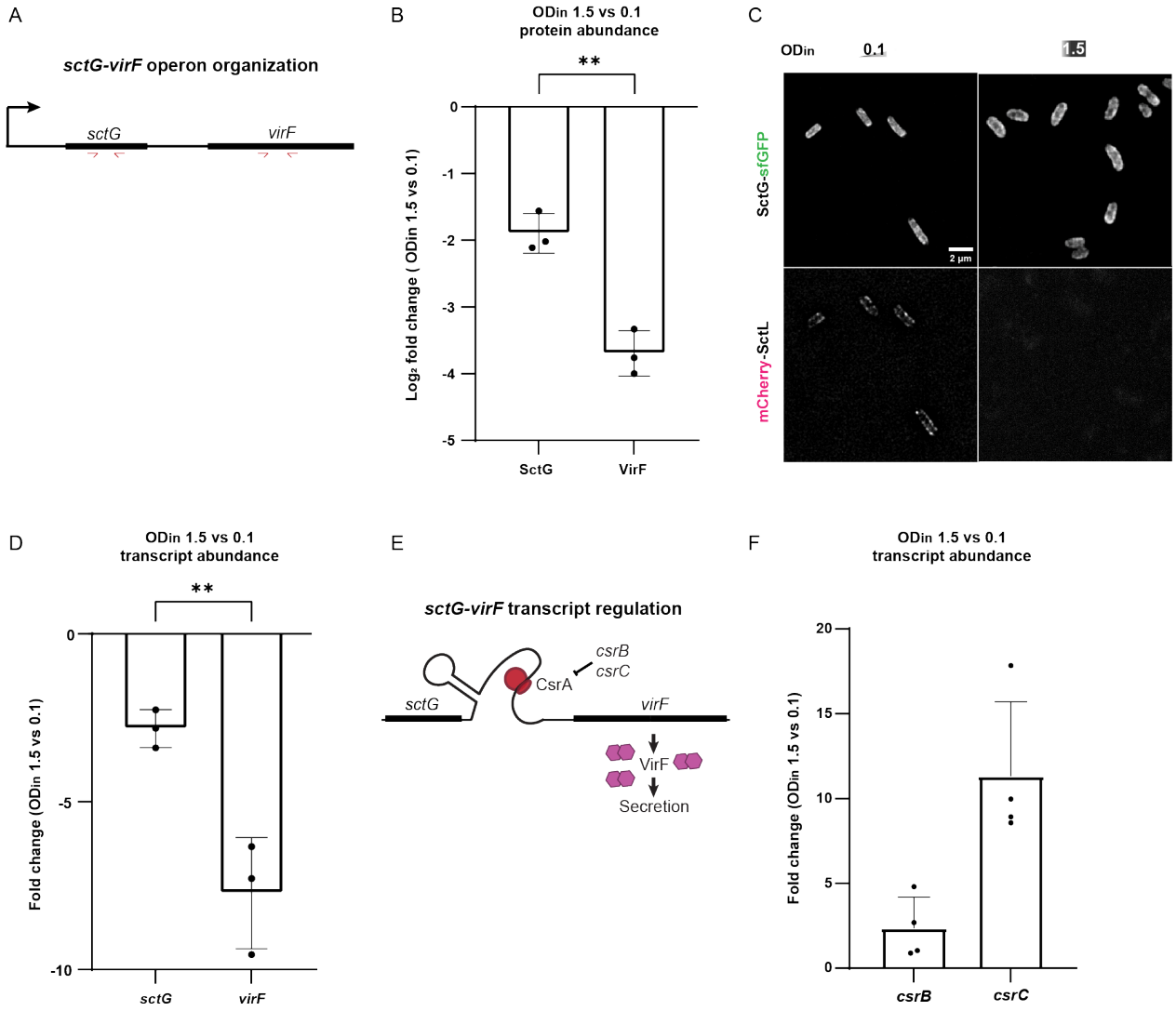

Fig. 5 – Bacterial density governs T3SS activity via posttranscriptional control of the *virF* transcript.

A) Organization of the *sctG-virF* operon, bold lines depict coding regions [18,63,66], red arrows indicate the position of RT-PCR primers. B) Protein levels of SctG and VirF at OD_{in} 1.5 vs. 0.1 (displayed as log_2 fold change), as measured by quantitative proteomics. C) Fluorescence microscopy of SctG-sfGFP (top) and the VirF-dependent T3SS component mCherry-SctL, both expressed from their native genetic background, at OD_{in} = 0.1 (left) or 1.5 (right). *n*=3, micrographs display representative results. D) Transcript levels of *sctG* and *virF* at OD_{in} 1.5 vs. 0.1, as measured by reverse transcriptase quantitative PCR (see panel A). E) Schematic depiction of the influence of the CsrABC system on VirF production [24,47,67]. The regulatory RNAs *csrB* and *csrC* sequester CsrA, preventing it from binding and stabilizing the *virF* transcript. F) Transcript levels of *csrB* and *csrC* at OD_{in} 1.5 vs. 0.1, as measured by reverse transcription quantitative PCR. In B), D) and F) small circles indicate individual biological replicates, whiskers denote standard deviation. **, $p<0.01$.

Host-cell adhesion is affected by cell density

Adhesion to host cells is a key virulence factor for many bacterial pathogens and a prerequisite for the utilization of the T3SS. Accordingly, the trimeric *Yersinia* adhesin YadA, which is co-encoded with the T3SS on the pYV virulence plasmid, is also regulated by VirF [68,69]. In line with this co-regulation, total proteome analysis showed a strong downregulation of YadA at higher cell densities (OD_{in} 1.5) (31.3-fold, $p<10^{-6}$) (Fig. 6A). To test whether this downregulation leads to a decreased adhesion to eukaryotic cells, which might promote the detachment and dissemination of bacteria at later stages of infection, we performed a host-cell attachment assay. Indeed, bacteria incubated at higher densities prior to the assay attached significantly less than the reference (OD_{in}= 0.1); the reduction almost mimicked the behavior of bacteria lacking *yadA*, which were used as a control (Fig. 6B).

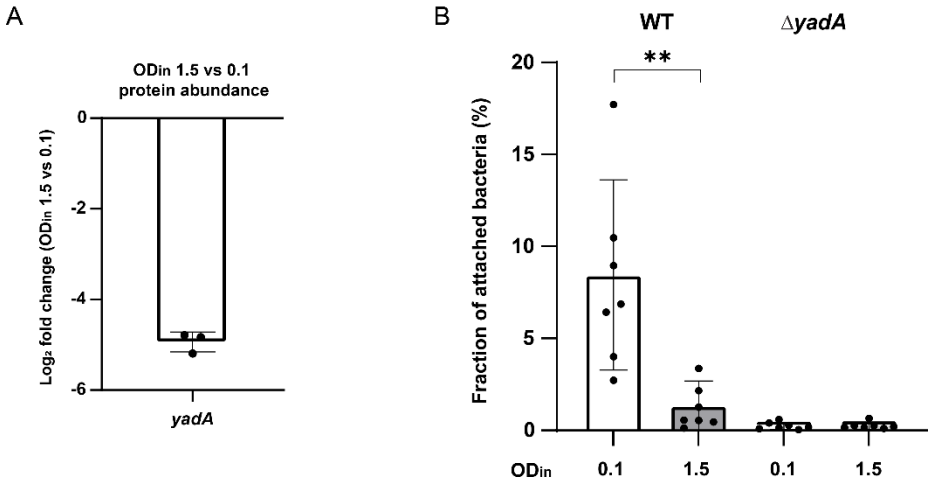

Fig. 6 – Host-cell adhesion is significantly downregulated at higher cell densities.

A) Protein levels of YadA at OD_{in} 1.5 vs. 0.1, as measured by quantitative proteomics. Small circles indicate individual biological replicates, whiskers denote standard deviation. *n*=3. B) Attachment of wild-type (WT) or *ΔyadA* bacteria at the conditions indicated (OD_{in} =0.1, 1.5) to HeLa cells (displayed as fraction of attached bacteria). Small circles indicate individual biological replicates, whiskers denote standard deviation, **, $p<0.01$.

Discussion

To establish an infection, bacterial pathogens initially need to enter the host organism and defend themselves against the host immune system on the way to their replication niches. However, after this initiation of infection, it is equally important for the bacteria to propagate in their niches and disseminate to other areas of the host organism or other hosts, a step that is often less appreciated and understood. The T3SS is a major virulence factor of important bacterial pathogens including *Salmonella*, *Shigella*, *Yersinia* and pathogenic *E. coli*. Its role in the establishment of infections is well-characterized and includes the uptake and inflammation establishment in *Salmonella* [70], phagocytosis and inflammation inhibition in *Yersinia* and *Shigella* [71,72], and actin pedestal formation and colonization in pathogenic *E. coli* [73]. However, presence of the T3SS may become an obstacle in the later steps of infection, because T3SS activity severely restricts bacterial growth and division across all main T3SS model organisms, including

Yersinia [26,27], *Salmonella* [32], and *Shigella* [34,74]. In this study, we set out to study this important point by investigating the formation and activity of the *Y. enterocolitica* T3SS across different bacterial densities, which may represent different stages of a bacterial infection. We found that *Yersinia* actively downregulates T3SS expression, assembly and activity at higher local densities. This contrasts with the previous picture of a completely T3SS-positive *Yersinia* population obtained from studies that focused on the initiation of an infection and therefore used lower cell densities [40,43,45–47,75]. Proteome analysis showed that the density-dependent T3SS downregulation is a highly specific phenotype that affects all T3SS components and the coregulated adhesion factor YadA, but very few non-T3SS-associated proteins (Fig. 2A, Table 1).

We found that the density-dependent downregulation of the T3SS is mediated by a pathway involving CsrABC and VirF, the main T3SS transcription factor in *Yersinia*. At higher bacterial densities, the regulatory protein CsrA, which usually stabilizes the *virF* transcript [47,65] is sequestered by higher concentrations of the regulatory RNAs *csrB* and *csrC.* This cascade leads to a gradual inhibition of the expression of VirF and, subsequently, all T3SS components, preventing the assembly of injectisomes and protein secretion by the T3SS. This regulatory pathway is a main factor in the density-dependent downregulation of the T3SS, which is highlighted by the finding that additional expression of VirF *in trans* at high bacterial densities restores T3SS activity.

The CsrABC (carbon storage regulator) system, originally identified as a glycogen synthesis regulator in *E. coli* [76], acts as a general regulator of bacterial virulence, motility, quorum sensing and biofilm formation via target mRNA transcript binding in many bacterial species [77–79]. Studies in *Y. pseudotuberculosis* showed that the CsrABC system strongly affects expression of the T3SS [24,47,67]. Similar to previous studies of CsrABC-based regulation of bacterial virulence, the precise upstream factors that convey the local bacterial density to the regulatory RNAs remain unclear. We experimentally tested the involvement of several candidates, namely quorum sensing (QS), the alternative sigma factor RpoS, and factors secreted into or depleted from the medium. There are several known links between QS and the T3SS, such as the inhibitory role of cell-cell communication on *Vibrio harveyi* and *P. aeruginosa* T3SS at high cell density [80,81]. Furthermore, Atkinson and colleagues provided evidence for a negative influence of QS on T3SS secretion in *Y. pseudotuberculosis* during biofilm formation in *Caenorhabditis elegans* [82]. However, we found that a *Y. enterocolitica* strain lacking both known QS systems still retained the d^3T3 (Fig. 3A). This lack of influence of the QS on d^3T3 is in line with previous studies showing no effect of QS on *Y. enterocolitica* T3SS regulation [56,58]. Similarly, we neither observed a significant down-regulation of T3SS activity in spent medium previously incubated at higher densities, nor a recovery of activity at high densities upon provision of fresh medium (Fig. 2BC), showing that any potential factor in the medium that might control T3SS activity would be short-lived. Finally, consistent with the distinct and specific nature of the phenotype, deletion or overexpression of RpoS had no influence on the d^3T3 (Fig. 3B).

The T3SS is an essential virulence factor for many of the pathogenic bacteria that employ it, such as *Salmonella*, *Shigella* and *Yersinia*. However, its presence and activity are a double-edged sword: While the T3SS allows to manipulate host cells and in this way to evade the immune response (reviewed in [83]), or to ensure the bacterial entry into target cells (reviewed in [74]), its activity severely restricts the bacterial ability to multiply. Accordingly, assembly and activity of the T3SS are tightly regulated. A striking example is the bimodal expression of the SPI-1 T3SS in *Salmonella enterica*, where the inflammation caused by the activity of the T3SS in a fraction of bacteria leads to a clearing of bacterial competitors, allowing the T3SS-negative siblings to fill the resulting niche [32,84,85]. A similar effect was previously not observed for *Yersinia*, which is uniformly T3SS-positive at the low densities used for most laboratory experiments [40,45–47]. This could be rationalized by the fact that, like in *Shigella*, the T3SS mainly provides an individual advantage by phagocytosis and inflammation inhibition [75,86,87]. However, like other bacteria, *Yersinia* needs to propagate in its niche. We hypothesize that the d^3T3, described in this study, allows this propagation and the subsequent spreading of bacteria at higher local bacterial densities. Mouse infection experiments confirmed that bacterial densities in several organs steeply rise at later stages of infection (e.g. by about 100-fold between day 2 and day 5 [88]), suggesting that this phenotype may well be relevant during infection. The resulting complete downregulation of expression and assembly of the T3SS components ensures that the T3SS cannot be unspecifically activated upon contact to eukaryotic cells during this later phase of the infection.

A key aspect of the d^3T3 is that besides all components of the T3SS, it also affects YadA, the trimeric autotransporter adhesin mediating the adhesion to extracellular matrix components of eukaryotic host cells [69,89,90], which is also part of the VirF regulon. As shown in Fig. 6, this downregulation has a striking effect on bacterial attachment, allowing bacteria to detach from eukaryotic cells and preventing reattachment during dissemination (Fig. 7). Importantly, the reversibility of the d^3T3 (Fig. 2B) ensures that once bacteria are in a site with a lower local bacterial concentration, the T3SS can be reassembled, a process that takes 30-60 minutes [42], sufficient to disseminate in or between hosts, but ensuring that the T3SS is ready for the establishment of a fresh infection cycle at the new site.

In summary, we show that contrary to what was previously believed*, Y. enterocolitica* downregulates the expression of its T3SS and the associated adhesin YadA at higher bacterial densities. This specific downregulation is conveyed by the CsrABC system via the main T3SS transcription factor VirF: increased levels of the regulatory RNAs *csrB* and especially *csrC* at higher local densities sequester CsrA and thereby destabilize the *virF* transcript. The resulting T3SS- and YadA-negative population can multiply and disseminate, even in the presence of potential target cells, an important aspect of bacterial virulence. Future experiments may reveal whether similar mechanisms ensure efficient replication and dissemination of *Shigella* and other T3SS-utilizing pathogens.

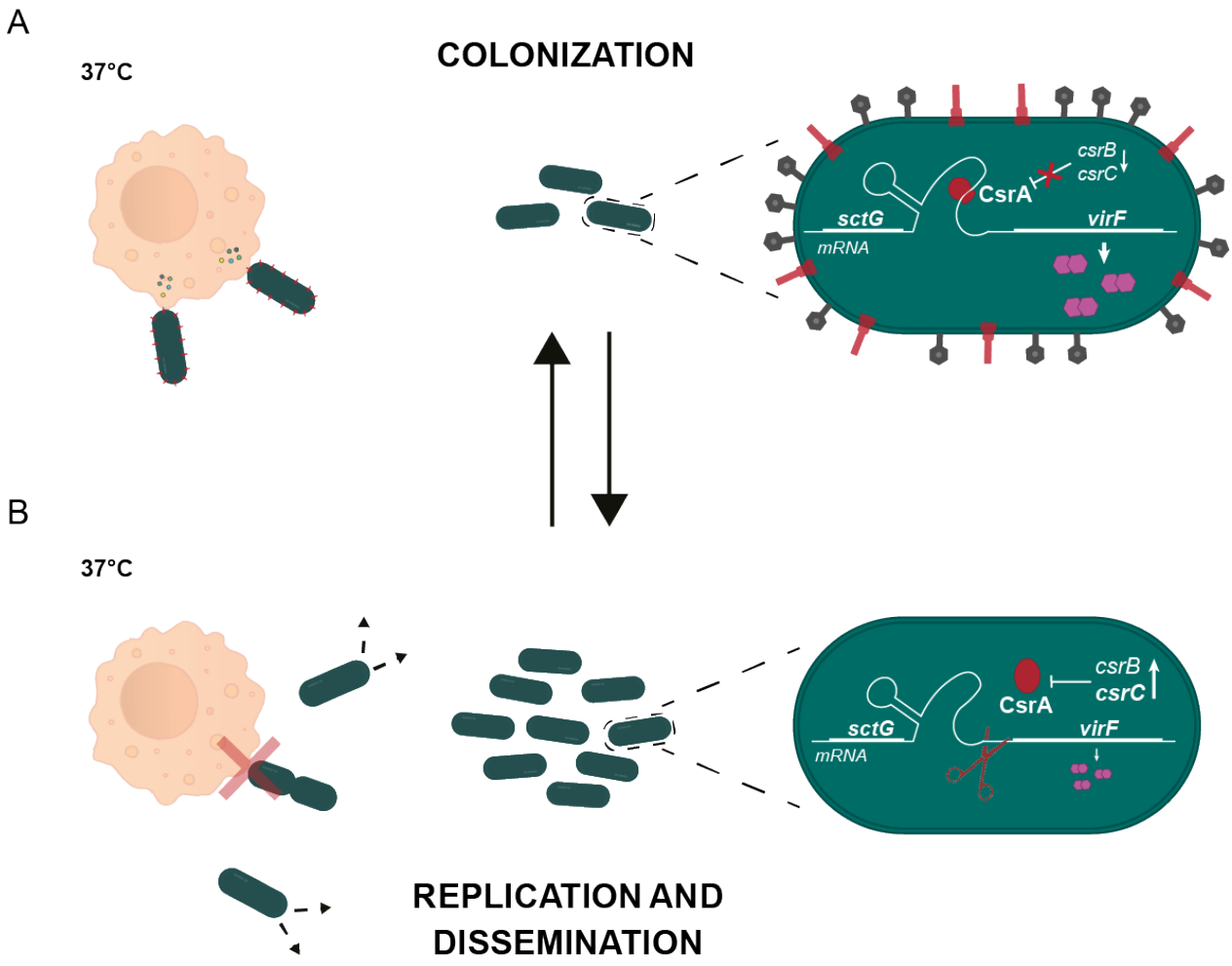

Fig. 7 – Influence of local higher cell density on T3SS secretion and on host-cell attachment.

A) At lower cell densities, *Yersinia* relies on the adhesion protein YadA (depicted in grey on the bacterial surface) and effector secretion by the T3SS (depicted in red on the bacterial surface) to colonize the host by fighting the host immune system. Both adhesion and secretion are regulated by the transcription factor VirF. Upon host entry, sensed as 37°C shift, the *virF* transcript is stabilized thanks to the global mRNA regulator CsrA. The efficient binding of CsrA to *virF* and resulting expression of T3SS components are ensured by the low basal levels of the two CsrA inhibitory RNAs *csrBC* [24,47,67]. B) At higher local cell densities, increased *csrC* levels sequester CsrA, which causes a higher turnover of the *virF* transcript, leading to a decreased expression of T3SS components and YadA. The resulting decrease in adhesion and T3SS activity promotes *Yersinia* replication and dissemination at later stages of infection.

Materials & Methods

Bacterial strain generation and genetic constructs

A list of strains and plasmids used in this study can be found in Suppl. Table 3. The *Y. enterocolitica* strains used in this study are based on the *Y. enterocolitica* wild-type strain MRS40 or its derivate IML421asd (ΔHOPEMTasd). IML421asd lacks all major virulence effector proteins (YopH,O,P,E,M,T) and harbors a deletion in the aspartate-beta-semialdehyde dehydrogenase gene, making the strain auxotrophic for diaminopimelic acid (DAP) and therefore suitable for work in a biosafety class 1 environment [91].

Bacterial cultivation, secretion assay, and total protein assays

Y. enterocolitica overnight cultures were grown on a shaking incubator at 28°C in brain heart infusion medium (BHI) supplemented with nalidixic acid (Nal, 35 µg/ml) and DAP (60 µg/ml), where required. Day cultures (BHI supplemented with 35 µg/ml Nal, 60 µg/ml DAP, where required, 20 mM $MgCl_2$, 0.4% glycerol and 5 mM EGTA for secreting conditions or 5 mM $CaCl_2$ for non-secreting conditions) were inoculated from fresh stationary overnight cultures to an OD_{600} of 0.1, 0.3, 0.7, 1.0, or 1.5. To select for the maintenance of expression plasmids, ampicillin was added (0.2 mg/ml), where required. Day cultures were incubated at 28°C for 90 min after the inoculum. Expression of the *yop* regulon was then induced by a rapid temperature shift to 37°C. Where needed, protein expression from pBAD-His/B (Invitrogen) derivative plasmids was induced at the temperature shift by adding 0.01–0.2% L-arabinose, as described for the respective experiments. Bacteria were incubated for 150-180 min after 37°C shift. For secretion assays, 2 ml of the culture supernatant was harvested by centrifugation (10 min, 21,000 *g*). Proteins in the supernatant were precipitated with 10% trichloroacetic acid (TCA) at 4°C for 1-8 h. 15 min centrifugation (21,000 *g*, 4°C) was performed to collect precipitated proteins. After washing with ice-cold acetone (1 ml) the pellets were resuspended in SDS-PAGE loading buffer and normalized to 0.3 OD units (ODu) for total cell analysis, or 0.6 ODu for secretion assay (1 ODu = 1 ml of culture at OD_{600} of 1, ~ 5 x 10^8 *Y. enterocolitica*). After resuspension, samples were incubated for 5 min at 99°C. Protein separation was performed on 15% SDS-PAGE gels and protein size was determined using the BlueClassic Prestained Marker (Jena Biosciences) as standard. For visualization, the gels were stained with FastGene-Q-stain (NipponGenetics). Gel band intensity was quantified in Fiji [92] by measuring the single-band area. For immunoblots, the separated proteins were transferred to a nitrocellulose membrane. Primary mouse anti-GFP antibody (ThermoFisher Proteintech 66002-1-lg, 1:4000) was used in combination with a secondary anti-mouse antibody conjugated to horseradish peroxidase (GE Healthcare NXA931, 1:5000). Primary rabbit anti-mCherry antibody (BioVision 5993 1:2000) was used in combination with a secondary anti-rabbit antibody conjugated to horseradish peroxidase (Sigma-Aldrich A8275 1:10 000). For visualization, Immobilon Forte chemiluminescence substrate (Sigma-Aldrich) was used in a LAS-4000 Luminescence Image Analyzer.

Growth curve and promoter activity assays

For cellular growth and measurements of T3SS activation via upregulation of the YopE promoter (P*yopE-sfGFP::ssrA*), bacteria were treated as described above. After 90 min at 28°C, bacterial cultures were aliquoted in quadruplicates into a 96-well microplate (120 µl/well). GFP fluorescence (excitation: 480/25 nm, emission: 535/28 nm) for P*yopE* assays and absorbance at 600 nm for growth curves were measured at 37°C over time in a Tecan Infinite 200 Pro photometer. The measured absorbance was converted into OD_{600} based on a calibration performed using the same culture volume and microtiter plate.

For sfGFP::ssrA degradation kinetics measurement, bacteria were treated as described before. After 120 min at 37°C in secreting-inducing conditions (5mM EGTA), T3SS induction was stopped by adding 10 mM Ca^{2+}. bacterial cultures were aliquoted in quadruplicates into a 96-well microplate (120 µl/well). The sfGFP (480-535 nm) was measured at 37°C over time into a Tecan Infinite 200 Pro photometer.

Fluorescence Microscopy

For fluorescence microscopy, bacteria were grown as described above. After 2.5 h at 37°C, 500 µl of culture were harvested (2400 *g* 2 min) and re-suspended in 250 µl of minimal medium (100 mM 2-[4-(2-Hydroxyethyl)piperazin-1-yl]ethane-1-sulfonic acid (HEPES) pH 7.2, 5 mM $(NH_4)_2SO_4$, 100 mM NaCl, 20 mM sodium glutamate, 10 mM $MgCl_2$, 5 mM K_2SO_4, 50 mM 2-(N-morpholino) ethane sulfonic acid (MES), 50 mM glycine). 2 µl of bacterial resuspension were spotted on an agarose pad (1.5% low melting agarose (Sigma-Aldrich) in minimal medium, 1% casamino acids, 5 mM EGTA, glass depression slides (Marienfeld)). For imaging, a Deltavision Elite Optical Sectioning Microscope equipped with a UPlanSApo 100×/1.40 oil objective (Olympus) and an EDGE sCMOS_5.5 camera (Photometrics) was used. z stacks with 9 slices (Δz = 0.15 µm) per fluorescence channel were acquired. GFP signal was visualized using a GFP filter set (excitation: 480/25 nm, emission: 535/28 nm) with 0.2 s exposure time. The mCherry signal was visualized using a mCherry filter set (excitation: 575/25 nm, emission: 625/45 nm) with 0.2 s exposure time. Images were processed with FIJI (ImageJ 1.51f/1.52i/1.52n) (Schindelin et al, 2012)(Schindelin et al, 2012). Fluorescence quantification was performed in FIJI. For visualization purposes, selected fields of view adjusted identically for brightness and contrast within the compared image sets are shown.

Quantification of fluorescent foci

To quantify the number of stable EGFP-SctQ foci, individual *Y. enterocolitica* cells were first segmented using the neural network StarDist [93]. The training dataset was generated by manually annotating 17 images of *Y. enterocolitica* cells grown in BHI medium and imaged on agarose pads using the Deltavision Elite Optical Sectioning Microscope. To account for variation in the imaging plane, z-stacks with 150 nm spacing were recorded, of which 5 slices were selected for network training. The resulting 85 images were quartered, resulting in a final dataset of 300 (training) and 40 (validation) image pairs. Dataset size was increased 4-fold during training using flipping and rotation. The StarDist model was trained for 100 epochs

via the ZeroCostDL4Mic platform [94] using a batch size of 4, 260 steps, 120 rays, grid size of 2, an initial learning rate of 0.0003 and an train/test split of 80%/20%. The dataset and model are included in the DeepBacs [95] collection on Zenodo (doi: 10.5281/zenodo.11105050). Foci localization was performed using the Fiji plugin ThunderSTORM [96]. Localizations were identified using 3rd order B-Spline filtering and local maximum approximation with a peak intensity threshold of 4-fold standard deviation of the 1st wavelet level. For sub-pixel localization, peaks were fitted with an integrated Gaussian in a fitting radius of 3 pixels. Finally, localizations were filtered by PSF width (sigma < 600 nm) and images were rendered as a scatter plot with a magnification of 1. This allows for foci counting by measuring the integrated intensity within the ROIs of segmented cells. To ensure that the foci are located within the cell outlines, each ROI was enlarged by 2 pixels with the help of a custom-written Fiji macro.

Proteome analysis by shotgun proteomics-based mass spectrometry

Strains were grown and prepared as described above. After 2.5 h at 37°C, cultures were normalized to an OD_{600} of 0.5, and 2 ml were harvested by centrifugation at 9,391 *g* for 2 min. The cells were washed three times with ice-cold phosphate-buffered saline (PBS) (8 g/l NaCl, 0.2 g/l KCl, 1.78 g/l Na_2HPO_4*2H2O, 0.24 g/l KH_2PO_4, pH 7.4) (15,000 *g*, 10 min, 4°C) and resuspended in 300 µl lysis buffer (2% sodium lauroyl sarcosinate (SLS), 100 mM ammonium bicarbonate). Then samples were heated for 10 min at 90°C and sonicated with a vial tweeter after heating. Proteins were reduced with 5 mM Tris(2-carboxyethyl) phosphine (Thermo Fischer Scientific) at 90°C for 15 min and alkylated using 10 mM iodoacetamid (Sigma Aldrich) for 30 min at 20°C in the dark. Proteins were precipitated with a 6-fold excess of ice cold acetone and incubation for 2h at -20°C, followed by two methanol washing steps. Dried proteins were reconstituted in 0.2% SLS and the amount of proteins was determined by bicinchoninic acid protein assay (Thermo Scientific). For tryptic digestion 50 µg protein was incubated in 0.5% SLS and 1 µg of trypsin (Serva) at 30°C over night. After digestion, SLS was precipitated by adding a final concentration of 1.5% trifluoroacetic acid (TFA, Thermo Fisher Scientific). Peptides were desalted by using C18 solid phase extraction cartridges (Macherey-Nagel). Cartridges were prepared by adding acetonitrile (ACN), followed by equilibration with 0.1% TFA. Peptides were loaded on equilibrated cartridges, washed with 5% ACN and 0.1% TFA containing buffer and finally eluted with 50% ACN and 0.1% TFA. Dried peptides were reconstituted in 0.1% Trifluoroacetic acid and then analyzed using liquid-chromatography-mass spectrometry carried out on an Exploris 480 instrument connected to an Ultimate 3000 RSLC nano and a nanospray flex ion source (all Thermo Scientific). The following separating gradient was used: 94% solvent A (0.15% formic acid) and 6% solvent B (99.85% acetonitrile, 0.15% formic acid) to 25% solvent B over 40 min, and an additional increase of solvent B to 35% for 20 min at a flow rate of 300 nl/min. MS raw data was acquired on an Exploris 480 (Thermo Scientific) in data independent acquisition (DIA) mode with a method adopted from [97]. The funnel RF level was set to 40. For DIA experiments full MS resolutions were set to 120.000 at m/z 200 and full MS, AGC (Automatic Gain Control) target was 300% with an IT of 50 ms. Mass range was set to 350–1400. AGC target value for fragment spectra was set at 3000%. 45 windows of 14 Da were used with an

overlap of 1 Da. Resolution was set to 15,000 and IT to 22 ms. Stepped HCD collision energy of 25, 27.5, 30% was used. MS1 data was acquired in profile, MS2 DIA data in centroid mode. Analysis of DIA data was performed using the DIA-NN version 1.8 [98] using a *Yersinia enterocolitica* GenBank protein database (https://www.ncbi.nlm.nih.gov/nuccore/NZ_CP011286.1) to generate a dataset-specific spectral library for the DIA analysis. The neural network based DIA-NN suite performed noise interference correction (mass correction, RT prediction and precursor/fragment co-elution correlation) and peptide precursor signal extraction of the DIA-NN raw data. The following parameters were used: Full tryptic digest was allowed with two missed cleavage sites, and oxidized methionine and carbamidomethylated cysteine residues. Match between runs and remove likely interferences were enabled. The precursor FDR was set to 1%. The neural network classifier was set to the single-pass mode, and protein inference was based on genes. Quantification strategy was set to any LC (high accuracy). Cross-run normalization was set to RT-dependent. Library generation was set to smart profiling. DIA-NN outputs were further evaluated using the SafeQuant [99,100] script modified to process DIA-NN outputs. The mass spectrometry proteomics data have been deposited to the ProteomeXchange Consortium via the PRIDE partner repository with the dataset identifier PXD052013 and can be accessed upon publication of the manuscript..

Sequence analysis

The CsrB and CsrC genetic regions of *Y. enterocolitica* KNG22703 (GenBank: CP011286.1) and *Y. pseudotuberculosis* YPIII (NZ_CP009792.1) [101] were compared. Alignments based on nucleotide sequence were performed by Clustal Omega.

RT-qPCR

Total RNA from *Y. enterocolitica* cells grown as described above was extracted using the Monarch Total RNA Miniprep Kit (New England Biolabs). A 10^9 cells pellet was first washed in cold-resuspension buffer (1 ml of 10 mM Tris-HCl pH 8.0, 100 mM NaCl, 1 mM EDTA), then resuspended cold-resuspension buffer (250 µl) and lysis buffer (250 µl of Tris/HCl pH 8 50 mM, Sucrose 8%, Triton X-100 1%, EDTA 10 mM, Lysozyme 0.4%) + 800 µL Monarch Total RNA Miniprep Kit protectant buffer and incubated for 30 min at 4°C. After incubation, cell resuspension was boiled for 15 min at 72°C. RNA purification was performed according to the manufacturer´s protocol. DNase treatment was performed using Turbo DNase (Thermo Fisher Scientific), followed by enzyme removal via Monarch RNA Cleanup Kit (New England Biolabs). cDNA was generated from 1 µg RNA using LunaScript RT SuperMix Kit (New England Biolabs). qPCR reactions were performed on an Applied Biosystems 7500 Real-Time PCR system using the Luna Universal qPCR MasterMix (New England Biolabs) and the primers listed in Suppl. Table 4. The DNA gyrase subunit *gyrB* was used as an internal control [102]. Data analysis was performed using the comparative threshold cycle (C_T) method [103].

Attachment assay

In preparation for the cell adhesion assay, HeLa cells were seeded and grown overnight in individual wells of 24-well cell culture plates (Grainer). Cells were incubated with fresh RPMI medium supplemented with DAP (60 µg/ml) before the addition of bacteria. After 2h in secretion-inducing conditions (37°C, 5 mM EGTA), approximately 5 x 10^6 bacteria were added to the PBS-washed HeLa monolayer (multiplicity of infection ~ 20) and incubated for 45 min. The attached cells were washed three times after incubation. HeLa cells and attached bacteria were collected via trypsinization and plated on *Yersinia* selective plates containing nalidixic acid (35 µg/ml) and DAP (60 µg/ml). After 24 h of incubation at 28°C, the number of colony-forming units was calculated per each condition tested.

Acknowledgement

The authors thank Johannes Schwabe for help with the RNA extraction and qPCR protocol and Katja Langenfeld for the support with cell culture experiments.

Table 1 – Density-dependent regulation of expression of T3SS components.

Label-free quantitative mass spectrometry of T3SS components in the total proteome of a ΔHOPEMTasd wild-type strain at the different growth conditions indicated. Proteins are sorted by the ratio of intensity at OD_{in} 1.5/OD_{in} 0.1 (red shades: downregulated at OD_{in} 1.5, blue shades: upregulated at OD_{in} 1.5), which the *p* values refer to as well. Exp.app., IM export apparatus; # pept., number of total detected peptides. Note that for some effectors, the mutations in the ΔHOPEMTasd strain allow the detection of a subset of peptides (Suppl. Table 4). *n.d.*, not detected; imputed values were used for the statistical analysis in these cases.

Protein	Log_2 intensity ratio	*p* value	Individual log_2 intensity values						# pept.
			OD_{in} = 0.1			OD_{in} = 1.5			
Rod / washer SctI	-8.00	6.9E-08	27.30	27.79	27.78	19.42	19.56	19.89	10
IM ring component SctD	-6.29	2.4E-05	29.83	29.83	29.89	22.59	23.72	24.38	20
Exp.app. component SctV	-6.24	2.3E-05	31.26	31.23	31.34	24.29	24.81	26.01	76
Exp.app. component SctR	-5.93	4.6E-07	25.81	25.83	25.98	*n.d.*	*n.d.*	*n.d.*	5
Effector YopO	-5.84	6.4E-06	31.16	31.23	31.24	24.63	25.83	25.65	25
Translocator SctE (YopB)	-5.53	5.3E-06	33.23	33.97	33.42	27.54	28.04	28.44	39
Needle subunit SctF	-5.20	5.4E-08	30.92	30.91	30.93	25.68	25.52	25.96	13
Translocator SctA (LcrV)	-4.80	4.1E-07	33.40	33.35	33.39	28.29	28.56	28.90	58
Secretin / OM ring SctC	-4.66	2.6E-07	30.90	30.97	30.98	26.02	26.30	26.56	38
Regulator YscX	-4.59	5.4E-07	27.99	28.17	28.01	23.18	23.45	23.77	12
IM ring component SctJ	-4.59	9.2E-07	31.26	31.25	31.32	26.46	26.52	27.09	35
Chaperone YscE	-4.56	6.8E-09	29.74	29.73	29.92	25.25	25.17	25.29	13
Translocator SctB (YopD)	-4.54	7.4E-06	32.14	32.94	32.27	27.69	27.81	28.23	71
Chaperone YscB	-4.52	9.5E-07	30.65	30.60	30.78	25.83	26.15	26.49	13
Effector YopT	-4.48	7.4E-03	23.29	23.33	23.28	*n.d.*	16.56	*n.d.*	5
Chaperone YscG	-4.46	1.7E-07	29.24	29.19	29.29	24.59	24.70	25.04	8
Regulator LcrG	-4.25	1.9E-06	30.42	30.40	30.47	25.80	26.20	26.53	28
Chaperone SycT	-4.25	4.0E-07	24.33	23.33	23.41	*n.d.*	*n.d.*	*n.d.*	3
Cytosolic component SctK	-4.08	1.2E-06	28.67	28.68	28.75	24.39	24.58	24.90	18
Exp.app. component SctU	-3.94	2.4E-07	26.93	27.02	27.09	22.81	23.02	23.40	16
Cytosolic component SctL	-3.94	8.1E-07	29.00	29.06	29.12	24.90	25.13	25.33	16
Regulator YscY	-3.92	2.1E-06	26.31	26.29	26.40	22.55	22.09	22.60	5
Chaperone SycD	-3.87	1.6E-06	32.33	32.35	32.34	28.12	28.48	28.80	22
Transcriptional activator VirF (LcrF)	-3.70	4.7E-06	28.76	28.79	28.85	24.76	25.03	25.51	15
Cytosolic ATPase SctN	-3.56	1.1E-05	30.93	30.93	31.02	26.92	27.53	27.76	46
Effector YopQ	-3.54	1.3E-06	29.25	29.44	29.11	25.51	25.69	25.97	17
Chaperone SycN	-3.34	1.8E-07	29.71	29.65	29.97	26.39	26.42	26.51	9
Gatekeeper TyeA	-3.11	3.4E-08	29.16	29.16	29.20	25.99	26.02	26.19	9
Secreted protein YscH/YopR	-2.98	9.7E-07	27.09	27.10	26.92	24.00	23.88	24.27	5
Effector YopE	-2.47	5.2E-04	24.95	24.83	25.09	22.73	21.76	22.96	6
Needle length regulator / ruler SctP	-2.40	2.3E-05	30.30	30.37	30.36	27.59	27.97	28.26	45
Cytosolic component SctO	-2.30	1.4E-04	25.40	25.39	25.39	22.63	23.10	23.55	9
Regulator LcrR	-2.27	5.2E-07	27.41	27.43	27.55	25.11	25.14	25.33	6
Chaperone SycE	-2.10	4.5E-06	30.09	30.15	30.11	27.84	27.96	28.25	8
Exp.app. component SctT	-2.09	1.5E-02	22.65	22.34	22.24	*n.d.*	*n.d.*	*n.d.*	4

Cytosolic component SctQ	-2.06	1.1E-04	29.58	29.58	29.63	27.10	27.71	27.82	13
Pilotin SctG (YscW)	-1.90	2.4E-05	28.46	28.44	28.39	26.35	26.41	26.83	9
Secreted gatekeeper SctW (YopN)	-1.73	3.8E-04	30.68	31.00	30.70	28.66	29.10	29.42	25
Chaperone SycH	-0.02	7.4E-01	29.65	29.63	29.66	29.57	29.55	29.75	21
Secreted neg. regulator YscM1	0.81	1.4E-02	27.53	27.52	26.86	28.34	28.06	27.93	11
Secreted neg. regulator YscM2	2.36	1.1E-05	26.01	26.07	25.96	28.64	28.40	28.09	9

References

[1] Cornelis. The type III secretion injectisome. Nat Rev Microbiol 2006.

[2] Deng W, Marshall NC, Rowland JL, McCoy JM, Worrall LJ, Santos AS, et al. Assembly, structure, function and regulation of type III secretion systems. Nat Rev Microbiol 2017;15:323–37.

[3] Galán JE, Wolf-Watz H. Protein delivery into eukaryotic cells by type III secretion machines. Nature 2006;444:567–73.

[4] Wagner S, Grin I, Malmsheimer S, Singh N, Torres-Vargas CE, Westerhausen S. Bacterial type III secretion systems: A complex device for the delivery of bacterial effector proteins into eukaryotic host cells. FEMS Microbiol Lett 2018;365.

[5] Bastedo DP, Lo T, Laflamme B, Desveaux D, Guttman DS. Diversity and evolution of type III secreted effectors: A case study of three families. Curr Top Microbiol Immunol, vol. 427, Springer Science and Business Media Deutschland GmbH; 2020, p. 201–30.

[6] Büttner D. Protein Export According to Schedule: Architecture, Assembly, and Regulation of Type III Secretion Systems from Plant- and Animal-Pathogenic Bacteria. Microbiology and Molecular Biology Reviews 2012;76:262–310.

[7] Jennings E, Thurston TLM, Holden DW. Salmonella SPI-2 Type III Secretion System Effectors: Molecular Mechanisms And Physiological Consequences. Cell Host Microbe 2017;22:217–31.

[8] Hüsing S, Halte M, van Look U, Guse A, Gálvez EJC, Charpentier E, et al. Control of membrane barrier during bacterial type-III protein secretion. Nat Commun 2021;12:3999.

[9] Kuhlen L, Abrusci P, Johnson S, Gault J, Deme J, Caesar J, et al. Structure of the core of the type iii secretion system export apparatus. Nat Struct Mol Biol 2018;25:583–90.

[10] Berger C, Ravelli RBG, López-Iglesias C, Kudryashev M, Diepold A, Peters PJ. Structure of the Yersinia injectisome in intracellular host cell phagosomes revealed by cryo FIB electron tomography. J Struct Biol 2021;213.

[11] Butan C, Lara-Tejero M, Li W, Liu J, Galán JE. High-resolution view of the type III secretion export apparatus in situ reveals membrane remodeling and a secretion pathway. PNAS 2019;12:24786–95.

[12] Hu B, Morado DR, Margolin W, Rohde JR, Arizmendi O, Picking WL, et al. Visualization of the type III secretion sorting platform of Shigella flexneri. Proc Natl Acad Sci U S A 2015;112:1047–52.

[13] Hu B, Lara-Tejero M, Kong Q, Galán JE, Liu J. In Situ Molecular Architecture of the Salmonella Type III Secretion Machine. Cell 2017;168:1065-1074.e10.

[14] Makino F, Shen D, Kajimura N, Kawamoto A, Pissaridou P, Oswin H, et al. The Architecture of the Cytoplasmic Region of Type III Secretion Systems. Sci Rep 2016;6.

[15] Diepold A, Kudryashev M, Delalez NJ, Berry RM, Armitage JP. Composition, Formation, and Regulation of the Cytosolic C-ring, a Dynamic Component of the Type III Secretion Injectisome. PLoS Biol 2015;13:e1002039.

[16] Diepold A, Sezgin E, Huseyin M, Mortimer T, Eggeling C, Armitage JP. A dynamic and adaptive network of cytosolic interactions governs protein export by the T3SS injectisome. Nat Commun 2017;8:15940.

[17] Wimmi S, Balinovic A, Brianceau C, Pintor K, Vielhauer J, Turkowyd B, et al. Cytosolic sorting platform complexes shuttle type III secretion system effectors to the injectisome in Yersinia enterocolitica. Nat Microbiol 2024;9:185–99.

[18] Böhme K, Steinmann R, Kortmann J, Seekircher S, Heroven AK. Concerted Actions of a Thermo-labile Regulator and a Unique Intergenic RNA Thermosensor Control Yersinia Virulence. PLoS Pathog 2012;8:1002518.

[19] Schwiesow L, Lam H, Dersch P, Auerbuch V. Yersinia Type III Secretion System Master Regulator LcrF. J Bacteriol 2016;198:604.

[20] Cambronne ED, Schneewind O. Yersinia enterocolitica type III secretion: yscM1 and yscM2 regulate yop gene expression by a posttranscriptional mechanism that targets the 5’ untranslated region of yop mRNA. J Bacteriol 2002;184:5880–93.

[21] Stainier I, Cornelis GR. YscM1 and YscM2, two Yersinia enterocolitica proteins causing downregulation of yop transcription. Mol Microbiol 1997.

[22] Allaoui A, Schulte R, Cornelis GR. Mutational analysis of the Yersinia enterocolitica virC operon: characterization of yscE, F, G, I, J, K required for Yop secretion and yscH encoding YopR. Mol Microbiol 1995;18:343–55.

[23] Kudryashev M, Diepold A, Amstutz M, Armitage JP, Stahlberg H, Cornelis GR. Yersinia enterocolitica type III secretion injectisomes form regularly spaced clusters, which incorporate new machines upon activation. Mol Microbiol 2015;95:875–84.

[24] Volk M, Vollmer I, Heroven AK, Dersch P. Transcriptional and Post-transcriptional Regulatory Mechanisms Controlling Type III Secretion. Curr Top Microbiol Immunol 2020;427:11–33.

[25] Heroven AK, Böhme K, Dersch P. The Csr/Rsm system of Yersinia and related pathogens: a post-transcriptional strategy for managing virulence. RNA Biol 2012;9:379–91.

[26] Kupferberg LL, Higuchi K. Role of calcium ions in the stimulation of growth of virulent strains of Pasteurella pestis. J Bacteriol 1958;76:120–1.

[27] Fowler JM, Wulff CR, Straley SC, Brubaker RR, Robert Brubaker CR. Growth of calcium-blind mutants of Yersinia pestis at 37 6C in permissive Ca 2+-deficient environments. Microbiology (Reading) 2009.

[28] Ben-Gurion R, Shafferman A. Essential virulence determinants of different Yersinia species are carried on a common plasmid. Plasmid 1981;5:183–7.

[29] Ferber DM, Brubaker RR. Plasmids in Yersinia pestis. Infect Immun 1981;31:839–41.

[30] Perry RD, Harmon PA, Bowmer WS, Straley SC. A Low-Ca2' Response Operon Encodes the V Antigen of Yersinia pestis. Infect Immun 1986;54:428–34.

[31] Michiels T, Wattiau P, Brasseur R, Ruysschaert JM, Cornelis G. Secretion of Yop proteins by yersiniae. Infect Immun 1990;58:2840–9.

[32] Sturm A, Heinemann M, Arnoldini M, Benecke A, Ackermann M, Benz M, et al. The cost of virulence: Retarded growth of salmonella typhimurium cells expressing type iii secretion system 1. PLoS Pathog 2011;7.

[33] Carter PB, Zahorchak RJ, Brubaker RR. Plague Virulence Antigens from Yersinia enterocolitica. vol. 28. 1980.

[34] Sasakawa C, Kamata K, Sakai T, Murayama SY, Makino S, Yoshikawa M. Molecular Alteration of the 140-Megadalton Plasmid Associated with Loss of Virulence and Congo Red Binding Activity in Shigella flexneri. vol. 51. 1986.

[35] Milne-Davies B, Helbig C, Wimmi S, Cheng DWC, Paczia N, Diepold A. Life After Secretion—Yersinia enterocolitica Rapidly Toggles Effector Secretion and Can Resume Cell Division in Response to Changing External Conditions. Front Microbiol 2019;10:2128.

[36] Diard M, Garcia V, Maier L, Remus-Emsermann MNP, Regoes RR, Ackermann M, et al. Stabilization of cooperative virulence by the expression of an avirulent phenotype. Nature 2013;494:353–6.

[37] Kroken AR, Chen CK, Evans DJ, Yahr TL, Fleiszig SMJ. The impact of ExoS on Pseudomonas aeruginosa internalization by epithelial cells is independent of fleQ and correlates with bistability of type three secretion system gene expression. MBio 2018;9:1–21.

[38] Lampaki D, Diepold A, Glatter T. A Serial Sample Processing Strategy with Improved Performance for in-Depth Quantitative Analysis of Type III Secretion Events in Pseudomonas aeruginosa. J Proteome Res 2020;19:543–53.

[39] Urbanowski ML, Brutinel ED, Yahr TL. Translocation of ExsE into Chinese hamster ovary cells is required for transcriptional induction of the Pseudomonas aeruginosa type III secretion system. Infect Immun 2007;75:4432–9.

[40] Wimmi S, Balinovic A, Jeckel H, Selinger L, Lampaki D, Eisemann E, et al. Dynamic relocalization of cytosolic type III secretion system components prevents premature protein secretion at low external pH. Nat Commun 2021;3:1625.

[41] Bajunaid W, Haidar-Ahmad N, Kottarampatel AH, Manigat FO, Silué N, Tchagang CF, et al. The t3ss of shigella: Expression, structure, function, and role in vacuole escape. Microorganisms 2020;8:1–28.

[42] Diepold A, Amstutz M, Abel S, Sorg I, Jenal U, Cornelis GR. Deciphering the assembly of the Yersinia type III secretion injectisome. EMBO Journal 2010;29:1928–40.

[43] Milne-Davies B, Helbig C, Wimmi S, Cheng DWC, Paczia N, Diepold A. Life After Secretion—Yersinia enterocolitica Rapidly Toggles Effector Secretion and Can Resume Cell Division in Response to Changing External Conditions. Front Microbiol 2019;10.

[44] Burgess JL, Case HB, Burgess RA, Dickenson NE. Dominant negative effects by inactive Spa47 mutants inhibit T3SS function and Shigella virulence. PLoS One 2020;15.

[45] Wiley DJ, Rosqvist R, Schesser K. Induction of the Yersinia Type 3 Secretion System as an All-or-None Phenomenon. J Mol Biol 2007;373:27–37.

[46] Cornelis G, Vanootegem J.-C, Sluiters C, Cornelis G. Transcription of the yop regulon from Y. enterocolitica requires trans acting pYV and chromosomal genes. Microb Pathog 1987;2:367–79.

[47] Kusmierek M, Hoßmann J, Witte R, Opitz W, Vollmer I, Volk M. A bacterial secreted translocator hijacks riboregulators to control type III secretion in response to host cell contact. PLoS Pathog 2019.

[48] Dewoody RS, Merritt PM, Marketon MM, Francis M, Forsberg A. Regulation of the Yersinia type III secretion system: traffic control. Front Cell Infect Microbiol 2013.

[49] Farrell CM, Grossman AD, Sauer RT. Cytoplasmic degradation of ssrA-tagged proteins. Mol Microbiol 2005;57:1750–61.

[50] Diepold A, Wagner S. Assembly of the bacterial type III secretion machinery. FEMS Microbiol Rev 2014;38:802–22.

[51] Hueck CJ. Type III Protein Secretion Systems in Bacterial Pathogens of Animals and Plants. vol. 62. 1998.

[52] Wagner S, Diepold A. A unified nomenclature for injectisome-type type III secretion systems. Curr Top Microb Immunol, vol. 427, 2020, p. 1–10.

[53] Bartra S, Cherepanov P, Forsberg Å, Schesser K. The Yersinia YopE and YopH type III effector proteins enhance bacterial proliferation following contact with eukaryotic cells. BMC Microbiol 2001;1:1–11.

[54] Badger JL, Miller VL. Role of RpoS in survival of Yersinia enterocolitica to a variety of environmental stresses. J Bacteriol 1995;177:5370–3.

[55] Guan J, Xiao X, Xu S, Gao F, Wang J, Wang T, et al. Roles of RpoS in Yersinia pseudotuberculosis stress survival, motility, biofilm formation and type VI secretion system expression. Journal of Microbiology 2015;53:633–42.

[56] Atkinson S, Sockett RE, Cámara M, Williams P. Quorum sensing and the lifestyle of Yersinia. vol. 8. 2006.

[57] Atkinson S, Chang C-Y, Sockett RE, Cámara M, Williams P. Quorum Sensing in Yersinia enterocolitica Controls Swimming and Swarming Motility. J Bacteriol 2006;188:1451–61.

[58] Ng Y-K, Grasso M, Wright V, Garcia V, Williams P, Atkinson S. The Quorum Sensing System of Yersinia enterocolitica 8081 Regulates Swimming Motility, Host Cell Attachment, and Virulence Plasmid Maintenance. Genes (Basel) 2018.

[59] Axler-Diperte GL, Stewart HJ, Wren BW, Darwin AJ. YtxR Acts as an Overriding Transcriptional Off Switch for the Yersinia enterocolitica Ysc-Yop Type 3 Secretion System §. J Bacteriol 2009;191:514–24.

[60] Li L, Yan H, Feng L, Li Y, Lu P. LcrQ Blocks the Role of LcrF in Regulating the Ysc-Yop Type III Secretion Genes in Yersinia pseudotuberculosis. PLoS One 2014;9:92243.

[61] Koster M, Bitter W, De Cock H, Allaoui AA, Cornelis GR, Tommassen J. The outer membrane component, YscC, of the Yop secretion machinery of Yersinia enterocolitica forms a ring-shaped multimeric complex. Mol Microbiol 1997.

[62] Rau R, Darwin AJ. Identification of YsaP, the pilotin of the Yersinia enterocolitica Ysa type III secretion system. J Bacteriol 2015;197:2770–9.

[63] Wimmi S, Fleck M, Helbig C, Brianceau C, Langenfeld K, Szymanski WG, et al. Pilotins are mobile T3SS components involved in assembly and substrate specificity of the bacterial type III secretion system. Mol Microbiol 2024;2:304–23.

[64] Liu L, Huang S, Fei K, Zhou W, Chen S, Hu Y. Characterization of the binding motif for the T3SS master regulator LcrF in Yersinia pseudotuberculosis. FEMS Microbiol Lett 2021;368:31.

[65] Ozturk G, Legrand K, Zheng Y, Young GM. Yersinia enterocolitica CsrA regulates expression of the Ysa and Ysc type 3 secretion system in unique ways. FEMS Microbiol Lett 2017;364:204.

[66] Cornelis G, Sluiters C, Lambert de Rouvroit C, Michiels T. Homology between virF, the transcriptional activator of the Yersinia virulence regulon, and AraC, the Escherichia coli arabinose operon regulator. J Bacteriol 1989;171:254–62.

[67] Kusmierek M, Dersch P. Regulation of host-pathogen interactions via the post-transcriptional Csr/Rsm system. Curr Opin Microbiol 2018;41:58–67.

[68] El Tahir Y, Skurnik M. YadA, the multifaceted adhesin. Int J Med Microbiol 2001;8:209–18.

[69] Mühlenkamp M, Oberhettinger P, Leo JC, Linke D, Schütz MS. Yersinia adhesin A (YadA) - Beauty & beast. International Journal of Medical Microbiology 2015;305:252–8.

[70] Galán JE. Salmonella interactions with host cells: type III secretion at work. Annu Rev Cell Dev Biol 2001;17:53–86.

[71] Cornelis GR, Gijsegem F Van. ASSEMBLY AND FUNCTION OF TYPE III SECRETORY SYSTEMS. vol. 54. 2000.

[72] Sansonetti PJ. themes Microbes and Microbial Toxins: Paradigms for Microbial-Mucosal Interactions III. Shigellosis: from symptoms to molecular pathogenesis. 2001.

[73] Celli J, Deng W, Finlay BB. Microreview Enteropathogenic Escherichia coli (EPEC) attachment to epithelial cells: exploiting the host cell cytoskeleton from the outside. Cell Microbiol 2000;2:1–9.

[74] Bajunaid W, Haidar-Ahmad N, Kottarampatel AH, Manigat FO, Silué N, Tchagang CF, et al. microorganisms The T3SS of Shigella: Expression, Structure, Function, and Role in Vacuole Escape. Microorganisms 2020.

[75] Milne-Davies B, Wimmi S, Diepold A. Adaptivity and dynamics in type III secretion systems. Mol Microbiol 2021;115:395–411.

[76] Sabnis NA, Yang H, Romeo T. Pleiotropic Regulation of Central Carbohydrate Metabolism in Escherichia coli via the Gene csrA. Journal of Biological Chemistry 1995;270:29096–104.

[77] Dubey AK, Baker CS, Romeo T, Babitzke P. RNA sequence and secondary structure participate in high-affinity CsrA-RNA interaction. RNA 2005.

[78] Mercante J, Edwards AN, Dubey AK, Babitzke P, Romeo T. Molecular Geometry of CsrA (RsmA) Binding to RNA and Its Implications for Regulated Expression. J Mol Biol 2009;392:511–28.

[79] Vakulskas CA, Potts AH, Babitzke P, Ahmer BMM, Romeo T. Regulation of Bacterial Virulence by Csr (Rsm) Systems. Microbiology and Molecular Biology Reviews 2015;79:193–224.

[80] Darshanee Ruwandeepika HA, Karunasagar I, Bossier P, Defoirdt T. Expression and Quorum Sensing Regulation of Type III Secretion System Genes of Vibrio harveyi during Infection of Gnotobiotic Brine Shrimp. PLoS One 2015.

[81] Waters CM, Wu JT, Ramsey ME, Harris RC, Bassler BL. Control of the type 3 secretion system in Vibrio harveyi by quorum sensing through repression of exsA. Appl Environ Microbiol 2010;76:4996–5004.

[82] Atkinson S, Goldstone RJ, Joshua GWP, Chang C-Y, Patrick HL. Biofilm Development on Caenorhabditis elegans by Yersinia Is Facilitated by Quorum Sensing-Dependent Repression of Type III Secretion. PLoS Pathog 2011;7:1001250.

[83] Cornelis GR. Mini-Review Yersinia type III secretion: send in the effectors. J Cell Biol 2002;158:401–8.

[84] Ackermann M, Stecher B, Freed NE, Songhet P, Hardt W-D, Doebeli M. Self-destructive cooperation mediated by phenotypic noise. Nature Letters 2008.

[85] Hautefort I, Proença MJ, Hinton JCD. Single-copy green fluorescent protein gene fusions allow accurate measurement of Salmonella gene expression in vitro and during infection of mammalian cells. Appl Environ Microbiol 2003;69:7480–91.

[86] Galán JE. Common Themes in the Design and Function of Bacterial Effectors. Cell Host Microbe 2009;5:571–9.

[87] Pha K. Yersinia type III effectors perturb host innate immune responses . World J Biol Chem 2016;7:1.

[88] Bent ZW, Branda SS, Young GM, Zachary Bent CW. The Yersinia enterocolitica Ysa type III secretion system is expressed during infections both in vitro and in vivo. Microbiologyopen 2013;2:962–75.

[89] Eltahir Y, Skurnik M. YadA, the multifaceted adhesin. International Journal of Medical Microbiology 2001;291:209–18.

[90] Tertti R, Skurnik M, Vartio T, Kuusela P. Adhesion protein YadA of Yersinia species mediates binding of bacteria to fibronectin. Infect Immun 1992;60:3021.

[91] Kudryashev M, Stenta M, Schmelz S, Amstutz M, Wiesand U, Castaño-Díez D, et al. In situ structural analysis of the Yersinia enterocolitica injectisome. Elife 2013;2:e00792.

[92] Schindelin J, Arganda-Carreras I, Frise E, Kaynig V, Longair M, Pietzsch T, et al. Fiji: an open-source platform for biological-image analysis. Nat Methods 2012;9:676–82.

[93] Schmidt U, Weigert M, Broaddus C, Myers G. Cell detection with star-convex polygons. Lecture Notes in Computer Science (Including Subseries Lecture Notes in Artificial Intelligence and Lecture Notes in Bioinformatics) 2018;11071 LNCS:265–73.

[94] von Chamier L, Laine RF, Jukkala J, Spahn C, Krentzel D, Nehme E, et al. Democratising deep learning for microscopy with ZeroCostDL4Mic. Nat Commun 2021.

[95] Spahn C, Gómez-de-Mariscal E, Laine RF, Pereira PM, von Chamier L, Conduit M, et al. DeepBacs for multi-task bacterial image analysis using open-source deep learning approaches. Communications Biology 2022 5:1 2022;5:1–18.

[96] Ovesny M, Kříž ek P, Borkovec J, ˇ vindrych ZS, Hagen GM. Bioimage informatics ThunderSTORM: a comprehensive ImageJ plug-in for PALM and STORM data analysis and super-resolution imaging. Bioinformatics 2014;30:2389–90.

[97] Bekker-Jensen DB, Martínez-Val A, Steigerwald S, Rü P, Fort KL, Arrey TN, et al. A Compact Quadrupole-Orbitrap Mass Spectrometer with FAIMS Interface Improves Proteome Coverage in Short LC Gradients Correspondence. Mol Cell Proteomics 2020;4:716–29.

[98] Demichev V, Messner CB, Vernardis SI, Lilley KS, Ralser M. Brief CommuniCation DIA-NN: neural networks and interference correction enable deep proteome coverage in high throughput. Nat Methods 2020.

[99] Glatter T, Ludwig C, Ahrné E, Aebersold R, Heck AJR, Schmidt A. Large-scale quantitative assessment of different in-solution protein digestion protocols reveals superior cleavage efficiency of tandem Lys-C/trypsin proteolysis over trypsin digestion. J Proteome Res 2012;11:5145–56.

[100] Ahrné E, Ahrné A, Molzahn L, Glatter T, Schmidt A. Critical assessment of proteome-wide label-free absolute abundance estimation strategies. Proteomics 2013;13:2567–78.

[101] Heroven AK, Böhme K, Rohde M, Dersch P. A Csr-type regulatory system, including small non-coding RNAs, regulates the global virulence regulator RovA of Yersinia pseudotuberculosis through RovM. Mol Microbiol 2008;68:1179–95.

[102] Avican K, Fahlgren A, Huss M, Heroven AK, Beckstette M, Dersch P, et al. Reprogramming of Yersinia from Virulent to Persistent Mode Revealed by Complex In Vivo RNA-seq Analysis. PLoS Pathog 2015;11:1–28.

[103] Schmittgen TD, Livak KJ. Analyzing real-time PCR data by the comparative CT method. Nature Protocols 2008 3:6 2008;3:1101–8.